SIMULATION OF NONEQUILIBRIUM HYPERSONIC BASE FLOW BEHIND SPACE VEHICLE

A.B. Gorshkov

Central Research Institute of Machine Building
141070, Korolev, Moscow region, Russia

One of the important problems in mathematical simulation of hypersonic flow around a spacecraft, entering the atmosphere of Earth or other planets with velocities greater than 3 km/s, is the study of nonequilibrium physical and chemical processes that occur in high-temperature shock layer around the vehicle.

During the flight of spacecraft in the atmosphere with the orbital or super-orbital velocity the gas temperature behind the shock wave in the nose region of the vehicle can reach a few thousand or tens of thousands of degrees. Under these conditions, high temperature processes such as vibrational excitation of molecules, dissociation, ionization and thermal radiation have a significant impact on the hot gas stream flowing around the spacecraft and, accordingly, on the aerodynamic characteristics and the magnitude of heat flux to its surface.

Currently, the rate constants of physical and chemical processes are not known with sufficient accuracy. They are determined either from laboratory experiments for the relatively low temperatures, or from theoretical calculations. The degree of applicability of these data for the conditions of the spacecraft entry in the atmosphere is unknown. Therefore, there arises the problem of verification of physical models and numerical methods used in the simulation of high-temperature flows by comparing the calculated results with experimental flight data. For the base region and the near wake behind the spacecraft the analysis of the flow is even more difficult when compared with the nose region of the vehicle, due to the formation of separation zones, lip and tail shocks, which lead to a complicated gas-dynamic flow pattern. This paper describes the results of parametric calculations of flow past a spacecraft for several points of a trajectory in the Earth's atmosphere, performed for the experimental reentry vehicle RAM-C [1].

Numerical method

In a sufficiently dense atmosphere, when the assumption of gas medium continuity is valid, a detailed analysis of flow and heat transfer parameters for the spacecraft flight can be made on the basis of numerical integration of the Navier-Stokes equations, supplemented by equations of mass conservation of the chemical species and energy conservation of the internal degrees of freedom. For solving the Navier-Stokes equations written in conservative form in an arbitrary coordinate system an implicit iteration scheme [2] is used which is a variant of the point Gauss-Seidel method. Details of the method are described in [3].

Thermo-chemical model of nonequilibrium air

To describe the nonequilibrium air flow a 9 species model is used [4]. The following chemical species are taken into account – N_2, O_2, NO, N, O, NO^+, N_2^+, O_2^+ and free electrons, for which there are three dissociation reactions, two exchange reactions and three reactions of associative ionization:

$$O_2 + M = O + O + M,$$

$$N_2 + M = N + N + M,$$

$$NO + M = N + O + M,$$

$$O + N_2 = N + NO,$$

$$O + NO = N + O_2,$$
$$N + N + M = N_2^+ + M,$$
$$O + O + M = O_2^+ + M,$$
$$N + O + M = NO^+ + M,$$

The vibrational temperatures of NO molecule and molecular ions N_2^+, O_2^+, NO^+ are assumed equal to the translational temperature. For N_2 and O_2 molecules vibrational energy conservation equations are solved (vibrational nonequilibrium model with three temperatures - T, T_{vN2}, T_{vO2}). Temperatures of free electrons and electronic excitation are supposed to be identical and equal to the vibrational temperature of nitrogen $T_e = T_{vN2}$. The rotational temperature of molecules is equal to the translational one. The vibration- dissociation interaction is taken into account according to the Marrone-Treanor model (CVDV) [5], parameter U of the model being equal to $E_D/3$, where E_D is dissociation energy of a molecule. Diffusion fluxes of i-th chemical species are defined according to Fick's law and have the form (in the direction of the x axis):

$$d_{i,x} = -\rho D_i \frac{\partial c_i}{\partial x}$$

Energy fluxes due to the vibrational heat conduction and diffusion of vibrationally excited molecules are:

$$J_{k,x}^{vib} = -\rho D_k \frac{\partial (c_k e_k^{vib})}{\partial x}, \quad k = N_2, O_2.$$

To determine the diffusion coefficients D_i the approximation of constant Schmidt numbers $Sc_i = \mu / \rho D_i$ is used, which are assumed equal to 0.75 for neutral particles. For the coefficients of ambipolar diffusion of ions the expression $D_i^{ion} = D_i (1 + T_e / T)$ is used. Total heat flux $\boldsymbol{q} = (q_x, q_y)$ is the sum of heat fluxes due to heat conduction and diffusion of chemical species:

$$q_x = -\kappa \frac{\partial T}{\partial x} + \sum_i h_i d_{i,x} + \sum_k J_{k,x}^{vib}$$

$$h_i = C_{p,i}^{tr} T + e_i^{el}(T_e) + e_i^{vib}(T) + h_{f,i}$$

where h_i, $h_{f,i}$, e_i^{el} – enthalpy, formation enthalpy and energy of electronic excitation of the i-th chemical species per unit mass, $e_i^{vib}(T)$, $i \neq N_2, O_2$ – the vibrational energy of the i-th molecular species, which is in thermodynamic equilibrium with translational temperature. The viscosity μ and thermal conductivity κ of the gas mixture are calculated with using Wilke's [6] and Mason-Saxena's [7] formulas.

On the vehicle surface the slip flow conditions are used – from [8] for the non-equilibrium air and from [9] for the perfect gas. The surface is assumed to be non-catalytic to neutral particles ($K_{i,w}$=0) and full catalytic for the ions:

$$d_{i,n} + K_{i,w} \rho_i = 0, \quad K_{i,w} = 0.5 \sqrt{\frac{2RT_e}{M_i}} \left(1 + \frac{T}{T_e}\right), \quad i = ion$$

where n is the normal to the surface.

Surface accommodation coefficients of the vibrational energy of molecules N_2 and O_2 are supposed to be zero. The surface temperature T_w in flight was variable, both along the vehicle and in

time. However, in the calculations from the methodological considerations T_w was set constant (400K). For comparison the calculations were also carried out at the same conditions for a perfect gas flow (ratio of specific heats $\gamma = 1.4$, viscosity was determined from the Sutherland formula for air).

Results

The RAM-C vehicle was a spherically blunted cone with a half-angle 9°, nose radius R_n = 0.1524 m and length L = 1.295 m. During the flight, in particular, measurements were carried out of peak electron density in the shock layer at several locations on the side of the vehicle, employing an effect of microwave radiation reflection. The calculations were performed with the use of non-equilibrium air and perfect gas models for three points of the RAM-C vehicle trajectory with parameters given in Table 1, where the index ∞ denotes a free stream value. Reynolds number Re_∞ is calculated from the free stream conditions and the radius of the vehicle base R_b.

Table 1. Trajectory parameters

H, km	V_∞, m/s	Re_∞	P_∞, atm	T_∞, K	C_{O2}	C_{N2}
61	7650	$4.71\cdot10^{4}$	$1.997\cdot10^{-4}$	244.2	0.234	0.766
71	7650	$1.36\cdot10^{5}$	$4.649\cdot10^{-5}$	217.0	0.234	0.766
81	7650	$3.23\cdot10^{3}$	$9.188\cdot10^{-6}$	196.3	0.234	0.766

Figure 1 shows the streamlines in the base region of the RAM-C vehicle at altitudes H = 61 and 81 km for the cases of non-equilibrium air (NA) and perfect gas (PG). The coordinates x and y are dimensionless and divided by R_b. The streamlines patterns and the configuration of separated zones at an altitude of 61 km for the models of non-equilibrium air and perfect gas differ slightly. The same situation takes place at an altitude of 71 km (the corresponding streamlines patterns, for brevity, are not shown in the figure), although the length of the separation region is reduced by about half. At an altitude of 81 km for perfect gas flow there is a small separation region of the size 0.2 – 0.3 the base radius R_b, while it is absent in the case of nonequilibrium air. This difference is explained by the stronger slip of flow along the base wall of the vehicle for nonequilibrium air, because the value of viscosity, calculated from the Wilke formula, is approximately 30% greater than the value of viscosity found from the Sutherland formula (under the flow conditions and at temperature on the outside boundary of the wall Knudsen layer of about T_s = 5000 – 6000 K).

Contours of isobars P/P_∞ in the shock layer at the aft of the side surface and in the base region of the RAM-C vehicle are depicted in Figure 2. On the side surface of the vehicle values of pressure for the models of non-equilibrium air and perfect gas are almost identical and are significantly

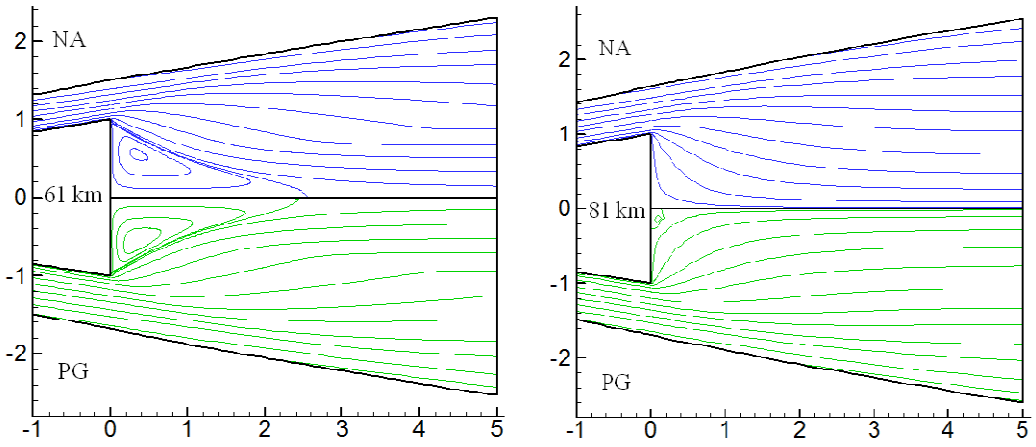

Fig. 1. Streamlines in base region of RAM-C vehicle at altitudes of 61 and 81 km.

increasing with altitude (approximately 1.5-fold), which is caused by the growing thickness of the boundary layer. In the near wake with diminishing altitude and the increasing role of physico-chemical processes, the difference in pressure levels for the two models of air increases. Pressure values on the base for non-equilibrium air are less than for perfect gas. The difference in the center of the base varies from 35% at an altitude of 61 km to 8% at an altitude of 71 km. A lower pressure in the near wake for nonequilibrium air at an altitude of 61 km is due to, as is evident from the Figure, a sharp drop in pressure in the rarefaction wave, which emanates from the corner edge (the values of P/P_∞ decreases from 16 at the beginning of the expansion wave to 1.5 and 2 for nonequilibrium air and perfect gas, respectively). This effect is explained by the higher values of the Mach number for the nonequilibrium air on the side surface (lower temperature), as well as greater adiabatic ratio (γ>1.4) due to the formation of atoms in dissociation. Note that, as calculations show, the processes of dissociation and vibrational relaxation in the rarefaction wave is almost completely frozen in this altitude range.

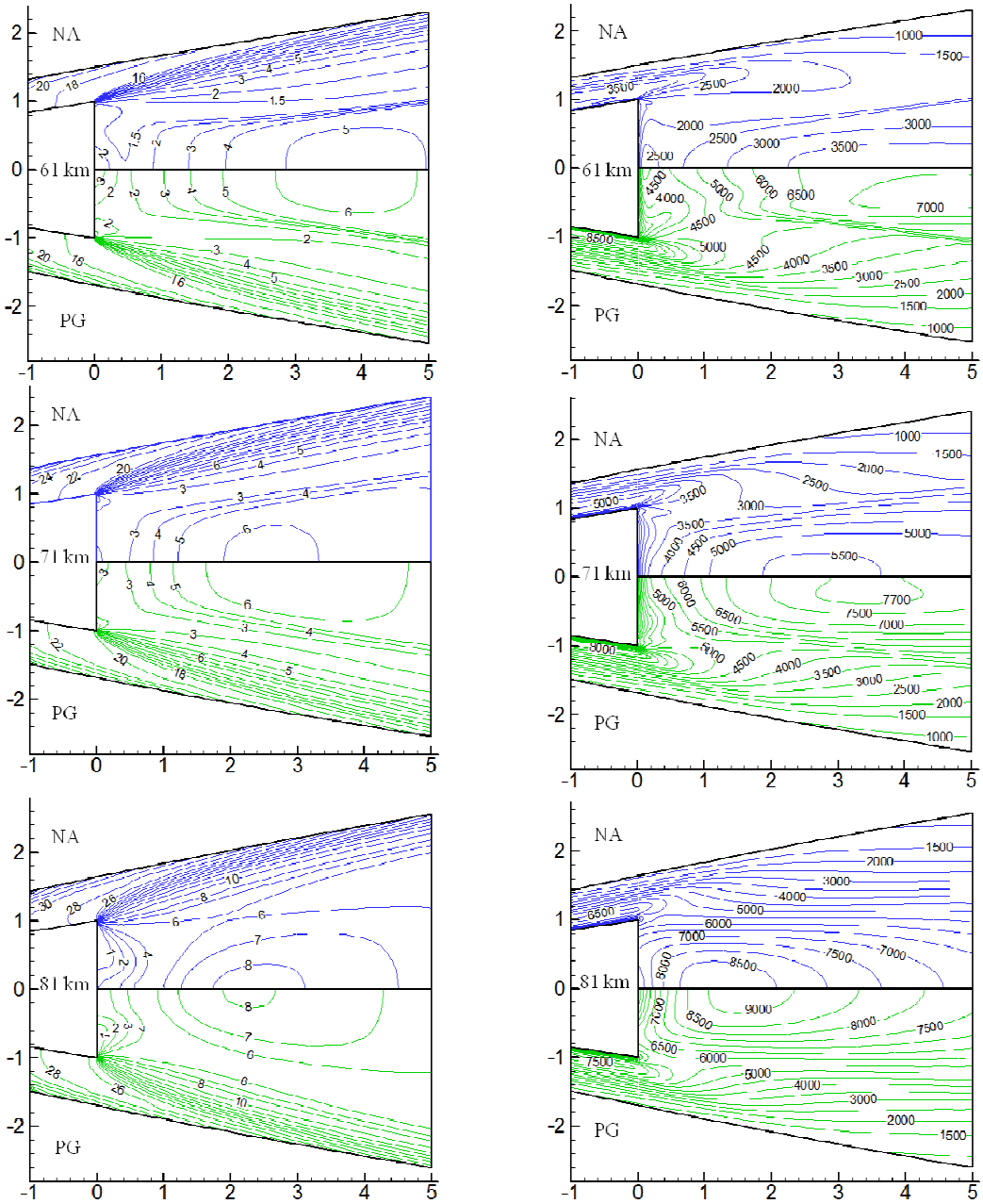

Fig. 2. Isobars P/P_∞ (left) and isotherms T,K in base region of RAM-C vehicle at 61, 71 и 81 km.

At high altitudes (81km), chemical reactions go very slowly, and the pressure in the near wake is almost independent of the model of air. The only exception is the vicinity of the vehicle base, where pressure for nonequilibrium air is less than for perfect gas (by 33% in the center of the base) due to, as mentioned above, the stronger slip of flow along the base wall and absence of the separation zone, which is observed for a perfect gas. With increasing altitude the transverse dimension of the rarefaction wave increases and the pressure drop P/P_∞ in it is reduced (from 8-10 at 61 km to about 4 times at 81 km), which is owing to the influence of viscosity.

As for pressure the difference of temperature levels in the near wake of RAM-C (Fig. 3) between the non-equilibrium air and perfect gas increases with decreasing altitude. At 81 km, where gas flow is nearly frozen, the temperature contours differ not considerably (no more than by 500 K), except for the vicinity of the base, where the effects of flow slip play the role. In contrast, at an altitude of 61 km, when the processes of dissociation and vibrational relaxation are important, the levels of temperature in the near wake for different models of air differ by approximately a factor of 2. On the side of the vehicle the difference of temperature levels is even more – 8500 K / 3500 K ≈ 2.4-fold. Note also that the maximum temperature value in the shock layer on the vehicle side surface for non-equilibrium air flow decreases with diminishing altitude, which is caused by an increase in the degree of gas dissociation. In perfect air flow the maximum temperature on the vehicle side, on the contrary, increases due to decrease of heat flux to the cold wall.

As seen from the isolines contours the positions of the T and P maxima in the base region are approximately the same and are located on the symmetry axis. The exception is the following two cases. At an altitude of 81 km (where there is no separation zone or it is very small) for both gas models the maximum of temperature on the symmetry axis is located much closer to the vehicle base than the maximum of pressure (particularly for nonequilibrium air flow – x = 1 and 2.2, respectively). At an altitude of 61 km the T maximum for perfect gas flow is observed at a certain distance ($y \approx 0.3$) from the symmetry axis and does not coincide with the P maximum, which is located on the symmetry axis at about the same distance from the base. It is interesting to note, that at high altitudes, 71 and 81 km for nonequilibrium air and 81 km for perfect gas, the temperature maximum in the near wake is greater than its maximum in the shock layer on the vehicle side. This is associated with an increase in the total enthalpy H_0 in the near wake with increasing altitude and the transition of the kinetic energy of the gas into the thermal energy in the base region, where the average gas velocity is less than on the side.

Isolines of the vibrational temperatures T_{vN2}, and T_{vO2} at three altitudes are shown in Figure 4. It is seen that T_{vO2} in the base region increases monotonically with decreasing altitude and reaches a very large (probably unrealistic) values of 18 000 K at an altitude of 61 km. This effect is a drawback of the Marrone-Treanor scheme and is caused by a relatively large supply of energy from recombination of the O atoms, which is not compensated by an energy exchange in the VT and VV' processes under conditions where molecular oxygen is almost completely dissociated ($C_{O2} \sim 10^{-6}$) and the energy contained in the vibrational mode of O_2 is small. Probably, in fact, the atom recombination does not occur mainly on the upper vibrational levels (as in Marrone-Treanor model), but on the electronically excited states of the molecule O_2, which are then quenched by collisions or spontaneous radiation. High T_{vO2} is also observed in the boundary layer on the blunt nose and the side surface. However, due to the low concentration of O_2 large values of T_{vO2} have no effect on the flow.

Unlike T_{vO2} the vibrational temperature of nitrogen T_{vN2} in the base region does not change monotonically and reaches a maximum of 5000 K at 71 km. Reduction of T_{vN2} at high altitudes is owing to the slowdown in VT and VV' processes, and at low altitudes – with the decrease of translational temperature due to more complete dissociation of the air. Since even at 61 km N_2 is not completely dissociated (approximately 30% - see Figure 4), the recombination of N atoms does not play such a significant role in the balance of the vibrational energy of N_2 as for O_2.

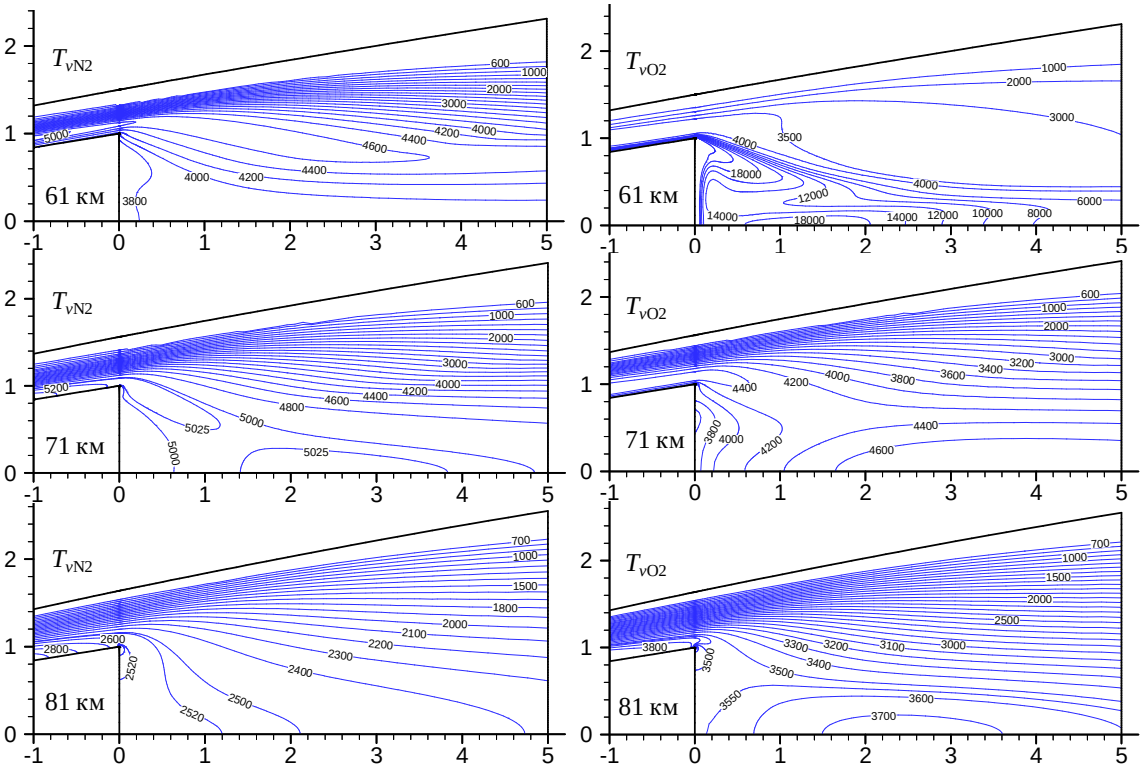

Fig. 3. Contours of vibrational temperatures of N_2 and O_2 – T_{vN2}, T_{vO2}, in base region of RAM-C vehicle.

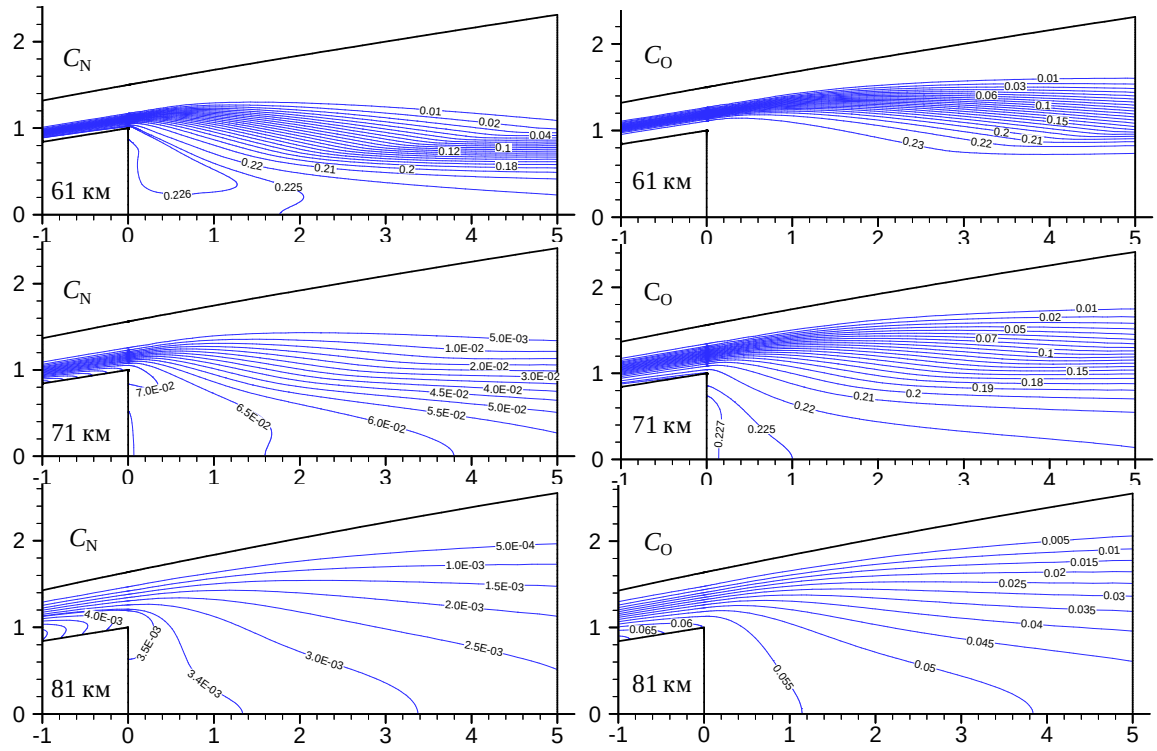

Fig. 4. Contours of mass fractions of N и O – $C_i=\rho_i/\rho$ in base region of RAM-C vehicle.

Figure 4 shows the isolines of the mass fractions C_i of N and O atoms in the base region at three altitudes. We see that at altitudes of 61 and 71 km O_2 dissociates completely, and N_2 – by 30% and 8% respectively. At an altitude of 81 km the degree of dissociation of O_2 in the base region is 24%, N_2 – 0.5%. In general one can note a slight change in the values of C_i in the near wake, although the concentration gradients increase with altitude. For example changes of mass

fractions along the symmetry axis within $5R_b$ from the base are growing from 2% to 32% for N and from 0.05 to 17% for O atoms with an increase in altitude from 61 to 81 km. Significant gradients at high altitudes are due to the diffusion processes, because chemical reactions under these conditions are almost frozen.

Figure 5 shows the calculated distribution of pressure and temperature along the symmetry axis in the near wake. At an altitude of 81 km, when the flow is frozen, the profiles of P and T for the non-equilibrium and perfect gas are quite close. A significant difference (1.5 times) is observed only near the vehicle base. It is caused by the mentioned difference in values of the gas viscosity calculated by the formulas of Wilke and Sutherland, which leads to a stronger slip and temperature jump on the surface for nonequilibrium air compared to perfect gas. With decreasing altitude, when the role of physico-chemical processes enlarges, the difference in the profiles of P and T for the two air models increases. Thus at an altitude of 61 km, the difference of temperatures reaches about 2 times, that of pressures – 30%. The difference of pressure values in the center of the base between non-equilibrium air and perfect gas does not vary monotonically with altitude. It is the lowest at an average altitude of 71 km, when the slip is small, and the physico-chemical processes are not strongly affect the flow. The same Figure also shows the calculated pressure values obtained in [10] using the Park model for nonequilibrium air. It is evident that there is good agreement with the results of the present calculation. The maximum difference is 10% for $x > 2$. Note that the pressure profile from [10] is smoother than in the present calculation, which is probably due to the coarser grid used in [10].

Figure 6 presents profiles of heat flux, pressure and temperature at the outer boundary of the wall Knudsen layer along the base of the RAM-C vehicle at three altitudes. For all the variables shown strong gradients (up to several times) take place along the base surface. An interesting feature of the heat flux profiles along the base at altitudes of 61 and 71 km is the presence of the second peak (in addition to one in the base center), regardless of air model. The position of the peak corresponds approximately to the separation point on the base surface. Note that at lower Mach numbers M_∞ = 8-12, and a rather high temperature factor $T_w/T_{0\infty} > 0.3$ this phenomenon was not observed [11, 12]. The values of heat flux and pressure in the center of the vehicle base for the both air models are shown in Table 2.

Table 2. Heat flux and pressure in the center of the vehicle base for two air models*

H, km	$q_w^{PG}/\rho_\infty V_\infty^3$	$q_w^{NA}/\rho_\infty V_\infty^3$	q_w^{PG}/q_w^{NA}	P^{PG}/P_∞	P^{NA}/P_∞	P^{PG}/P^{NA}
61	$2.55\cdot10^{-4}$	$9.96\cdot10^{-5}$	2.56	3.77	2.80	1.35
71	$3.09\cdot10^{-4}$	$2.05\cdot10^{-4}$	1.51	3.52	3.26	1.08
81	$7.13\cdot10^{-4}$	$6.82\cdot10^{-4}$	1.05	2.80	2.10	1.33

*PG/NA – perfect gas/ nonequilibrium air

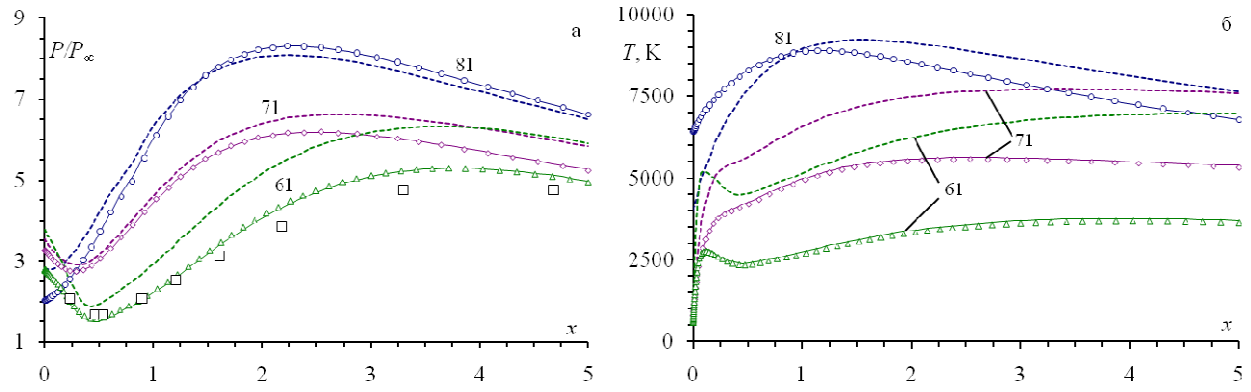

Fig. 5. Symmetry axis profiles of pressure and temperature at altitudes 61km (Δ), 71km (◊) and 81km (O) in the near wake of RAM-C vehicle. Points and solid lines – calculations on grids 70×70 and 100×100 (71, 81km), 100×100 and 140×140 (61km). Dotted lines – perfect gas calculations. Square markers – calculation results [10].

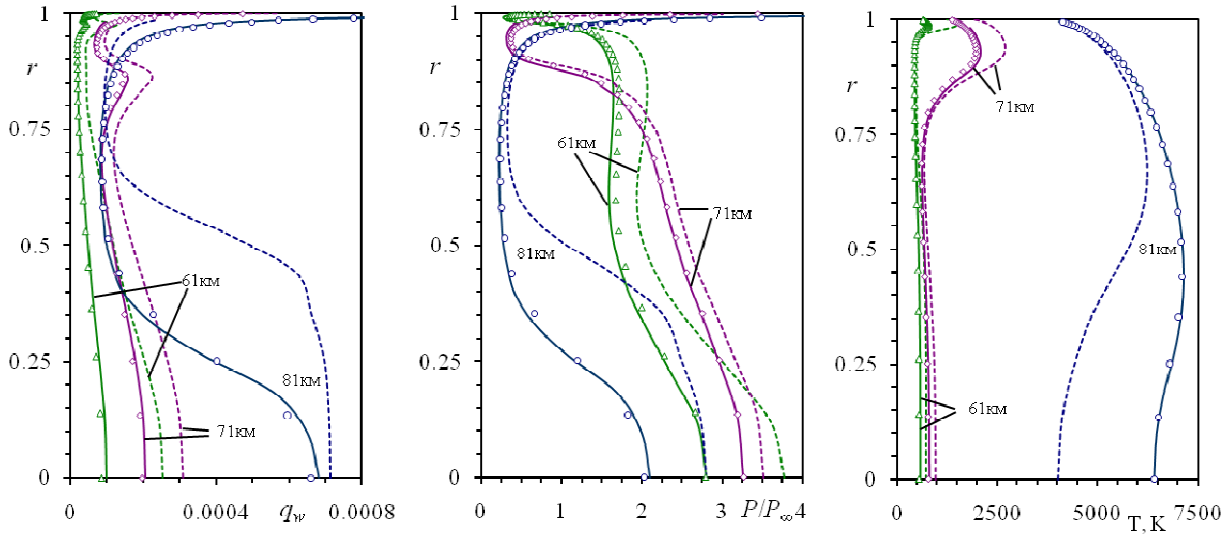

Fig. 6. Profiles of heat flux, pressure and temperature on outer boundary of wall Knudsen layer along the base of RAM-C vehicle at altitudes 61, 71 *и* 81 km. For other notation see Fig. 5.

As can be seen from Figure 6, taking into account non-equilibrium physical and chemical processes leads to a decrease in base heat flux and pressure (see also Table 2). The difference between heat fluxes in the base center q_w for the two air models diminishes monotonically with increasing altitude due to decrease of the role of physico-chemical processes. Large difference (approximately 2.5-fold) in the values of q_w at an altitude of 61 km is caused by a noncatalytical condition on the surface and the relatively frozen gas flow in the base region. Thus, for nonequilibrium air the major part of the energy of the free-stream flow near the cold base wall is remained deposited in the dissociation and excitation of internal degrees of freedom.

In contrast to heat flux the difference in base pressure for the two air models varies nonmonotonically with altitude and has the minimum at 71 km. With decreasing altitude, the base pressure difference grows because of the increasing role of physico-chemical processes, with increasing altitude – due to increasing influence of wall slip. Recall that the gas viscosity value, calculated using the Wilke formula, is larger than that found from the Sutherland formula. Therefore, flow slip and temperature jump on the base wall at 81km for nonequilibrium air is larger than that for perfect gas. At altitudes of 61 and 71 km sliding effect for nonequilibrium air, by contrast, is less because of lower temperatures and therefore higher density compared to the perfect gas flow.

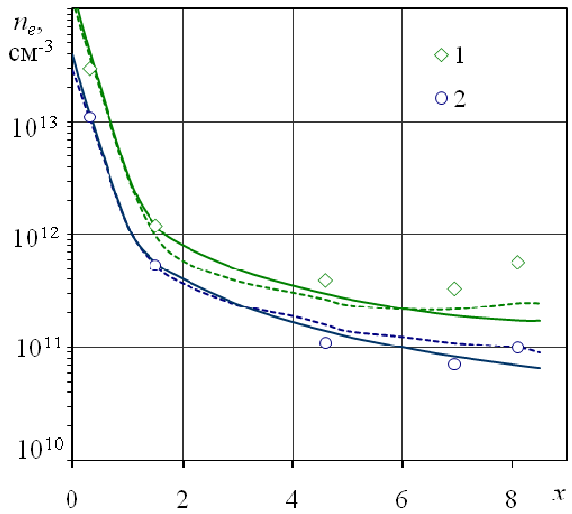

Fig. 7. Maximum values of electron density in shock layer over RAM-C vehicle. Points - experiment RAM-C [1] at altitudes of 61 (1) and 71 (2) km. Dotted and solid lines - calculation [10] and present calculation, respectively.

Figure 7 shows the theoretical (present calculation and results from [10]) and the experimental data for maximal electron density n_e in the shock layer on the side of the RAM-C vehicle depending on the distance along the axis from the nose stagnation point, referred to the radius of the nose bluntness R_n. There is a fairly good agreement between the calculated and experimental results, which become somewhat worse when approaching the base, where in the experiment (and to some extent in the calculations [10]) there is an incomprehensible rise in n_e.

Conclusion

Based on the numerical solution of the Navier – Stokes equations the effect of nonequilibrium physico-chemical processes has been investigated on the base pressure and heat transfer, separation zone size and other characteristics of the base region of a blunt cone for the flight conditions of experimental RAM-C vehicle in the altitude range 61 - 81 km. To verify the calculations the comparison was made with flight data on the electron density in the shock layer and with numerical results of other authors in the base region of the RAM-C vehicle.

Comparison of the calculation results, performed using the models of non-equilibrium air and perfect gas, showed that taking into account the real gas properties has the strongest influence on the base heat transfer and on the temperature in the base region, this effect being reduced with increasing altitude (more frozen flow). Effect of the real gas properties on the base pressure is smaller and varies non-monotonically with altitude. Streamlines patterns and separation zone size for the two air models differ insignificantly.

The present work was supported by Russian Foundation for Basic Research grant No. 12-01-00626a.

REFERENCES

1. **Grantham W.L.** Flight results of a 25,000 fps re-entry experiment: NASA TN D 6062. 1970.
2. **Jameson A., Yoon S.** A LU-SSOR scheme for the Euler and Navier-Stokes equations: AIAA Paper. 1987. № 87-0600. 11p.
3. **Gorshkov A.B.** Parallelization algorithm for implicit method computation of hypersonic nonequilibrium gas flow past a body, based on Navier–Stokes equations // Mathematical Models and Computer Simulations. 2010. Vol. 2, No. 2. P. 252-260 (in Russian: Matematicheskoe Modelirovanie. 2009. Vol. 21, No. 9, P. 43–53.).
4. **Vlasov V.I., Gorshkov A.B.** Comparison of the calculated results for hypersonic flow past blunt bodies with the OREX flight test data // Fluid Dynamics. 2001. Vol. 36, No. 5. P.812-819.
5. **Marrone P.V., Treanor C.E.** Chemical relaxation with preferential dissociation from excited vibrational levels // Phys. Fluids. 1963. Vol.6, No. 9. P. 1215-1221.
6. **Wilke C.** A viscosity equation for gas mixtures // J. Chem. Phys. 1950. Vol. 18, No. 4. P. 517-519.
7. **Mason E.A., Saxena S.C.** Approximate formula for the thermal conductivity of gas mixtures // Phys. Fluids. 1958. Vol. 1, No. 5. P. 361-369.
8. **Scott C.D.** Reacting shock layers with slip and catalytic boundary conditions // AIAA Journal. 1975. Vol. 13, No. 10. P. 1271-1278.
9. **Schaaf S.A., Chambre P.L.** Flow of rarefied gases // Fundamentals of Gas Dynamics / Ed. H.W.Emmons. N.J.: Princeton Univ. Press, 1958.
10. **Grasso F., Pirozzolli S.** Nonequilibrium effects in near-wake ionizing flows // AIAA Journal. 1997. Vol.35, No. 7. P. 1151-1163.
11. **Gorshkov A.B.** Calculation of base heat transfer behind thin cone-shaped bodies // Cosmonautics and Rocket Engineering. 1997. No.11. P. 13-20 (in Russian).
12. **Gorshkov A.B., Lunev V.V.** Laminar base flow downstream of slender cones in hypersonic flow // Fluid Dynamics. 2002. Vol. 37, No. 5. P. 772-783.